Mon. Not. R. Astron. Soc. **265,** 968–982 (1993)

Excited hydrogen and the formation of molecular hydrogen via associative ionization – I. Physical processes and outflows from young stellar objects

J. M. C. Rawlings,[1] J. E. Drew[1] and M. J. Barlow[2]
[1]*Department of Physics, Astrophysics, Nuclear Physics Laboratory, Keble Road, Oxford OX1 3RH*
[2]*Department of Physics and Astronomy, University College London, Gower Street, London WC1E 6BT*

Accepted 1993 June 28. Received 1993 June 9; in original form 1992 August 28

ABSTRACT

Rates for the associative ionization reaction $H(n=2)+H \rightarrow H_2^+ + e^-$ are calculated. This reaction is found to be a greater contributor to the H_2 formation rate than the direct radiative association reaction $H(n=2)+H \rightarrow H_2 + h\nu$ in most regions of astrophysical interest.

Chemical models of circumstellar regions are reassessed in the light of this information. We also examine the chemical behaviour of several other excited chemical species. A critical examination reveals that excitation effects are, in general, very important in many astrophysical situations and must be incorporated into the chemistry. H_2 has been detected in a variety of circumstellar regions and has a pivotal role in the overall chemistry. The method and efficiency of its formation are therefore of great importance.

We test the significance of the associative ionization reaction in several models. These models include a schematic description of the radiative transfer in H I Lyα. The endothermicity ($\simeq 1.1$ eV) of the reaction and the high departures from LTE that are required for the H I ($n=2$) level to be sufficiently populated restrict its significance to regions of high excitation, such as are found in circumstellar regions. In this paper (I), we investigate the importance of the reaction in winds associated with young stellar objects. In Paper II, the investigation will be extended to include novae, supernovae, planetary nebulae and shocked regions.

The results indicate that reactions involving excited atomic states may be very important in a number of circumstellar chemistries. Only exceptionally will reactions involving the higher excited states ($n>2$) be as significant as those involving $H(n=2)$.

Key words: molecular processes – circumstellar matter – stars: pre-main-sequence – ISM: jets and outflows – ISM: molecules.

1 INTRODUCTION

The chemistry of circumstellar and nebula regions, where temperatures and densities are high and the radiation field strong, differs greatly from that which is applicable to the general interstellar medium. In particular, the effect of the intense radiation fields and higher kinetic temperatures would be expected to inhibit the formation of H_2 severely. Yet there are examples of such environments where H_2 has been detected (e.g. in certain planetary nebulae). Since much of the rest of the chemistry involving other species is dependent on the H_2 abundance, it is in any case important that it is soundly modelled.

In this and a subsequent paper (Barlow, Rawlings & Drew, in preparation, hereafter Paper II), we take stock of the fundamental chemistry of hydrogen in a variety of circumstellar and nebular environments, paying particular attention to the role played by an associative ionization process, involving atomic hydrogen excited into the $n=2$ level, for which the cross-section has only recently become available (Urbain et al. 1991). By its nature, this is a process that will have greatest impact on H_2 formation in the near-stellar environments that we consider. In the present paper, we discuss the range of reactions likely to be important in the hydrogen chemistry, critically evaluating the available data, and assess the regimes in which the associative ionization

reaction and other excited-state processes may be efficient. We also deal with the specific example of the hydrogen chemistry in outflows from young stellar objects. A wider range of environments is considered in Paper II: we assess H_2 formation in old planetary nebulae, novae, supernovae and supernova remnants, and interstellar shocks. An early outline of the work described in both papers was presented by Rawlings, Drew & Barlow (1992).

The well-established pathways to H_2 formation in the gas phase are as follows. First, there is the direct three-body reaction:

$$H + H + H \rightarrow H_2 + H. \quad (1)$$

For this reaction to be significant, the density must typically be greater than about 10^{11} cm^{-3}. Such conditions are present, for example, in the early stages of a nova outburst (Rawlings 1988). At low densities and moderate ionization levels a much more efficient route is via the H^- ion:

$$H + e^- \rightarrow H^- + h\nu, \quad (2)$$

$$H^- + H \rightarrow H_2 + e^-. \quad (3)$$

This mechanism is believed to be the dominant H_2 formation route in many situations of interest (e.g. novae, Rawlings 1988; cool neutral winds, Glassgold, Mamon & Huggins 1989). However, the H^- ion can be lost by mutual neutralization,

$$H^- + H^+ \rightarrow H + H, \quad (4)$$

and is susceptible to photodetachment by the radiation field even at near-infrared wavelengths:

$$H^- + h\nu \rightarrow H + e^-. \quad (5)$$

In regions where there is a strong radiation field [and particularly in bright infrared sources, such as T Tauri stars (Rawlings, Williams & Cantó 1988)] this route is also suppressed.

Finally, as a 'last resort' the much less efficient H^+ route is the only apparent formation mechanism:

$$H^+ + H \rightarrow H_2^+ + h\nu, \quad (6)$$

$$H_2^+ + H \rightarrow H_2 + H^+. \quad (7)$$

However, the intermediate, H_2^+, is also susceptible to photodissociation and dissociative recombination:

$$H_2^+ + h\nu \rightarrow H^+ + H, \quad (8)$$

$$H_2^+ + e^- \rightarrow H + H. \quad (9)$$

In many of the previous studies it has not been common practice to take into proper account the internal excitation of the reacting chemical species. The excited electronic states of atomic species in general have very different chemical characteristics when compared to the ground state. For the molecular species, which can be excited rotationally, vibrationally and electronically, a variety of effects become important. Most notably, the cross-sections for photoreactions are highly excitation-dependent (as indeed is the case for reaction 8 above).

In many astrophysical environments of interest it is possible that significant fractions of chemical species are not in their ground state. If the relevant downward transitions are highly optically thick, then trapping may occur (as is often the case for H I Lyα) and the higher states may be well populated. In these circumstances Latter & Black (1991) proposed that H_2 formation may occur as a result of direct radiative association,

$$H + H(n=2) \rightarrow H_2 + h\nu. \quad (10)$$

The rate coefficient for this reaction was calculated to be $1.2/1.1 \times 10^{-14}$ cm^3 s^{-1} at 1000/10 000 K for the 2s channel and $3.4/4.2 \times 10^{-14}$ cm^3 s^{-1} at 1000/10 000 K for the 2p channel. Latter & Black pointed out that the reaction would have greatest effect where (i) H I Lyα trapping, or (ii) a recombination phase (in space or time) maintains an enhanced $H(n=2)$ population. They investigated three environments in which the required population enhancement would occur. These were the recombination era in the early Universe ($z > 1000$), diffuse H II regions and cool protostellar winds (as modelled by Glassgold et al. 1989). Only in the first of these did the new excited-state process make a palpable difference to the production of H_2.

We propose that a more efficient mechanism is provided by the associative ionization reaction,

$$H + H(n=2) \rightarrow H_2^+ + e^-, \quad (11)$$

which is followed by charge exchange with H (reaction 7) to form H_2. Although this again involves the unstable intermediate H_2^+, the measured cross-sections are substantially larger than those for the radiative association reaction. Hence it is possible that this second reaction involving the excited state is of wider significance.

In Section 2, we discuss the associative ionization reaction and the physical circumstances in which it might become significant. In Section 3, we reassess the known chemistry of hydrogenic species in hot, highly excited regions. Some additional reactions are discussed in Section 4 and, in Section 5, we make some general comments regarding the chemistry of non-hydrogenic species. In Section 6, we present models for winds from young stellar objects in which the new chemistry has been included and describe the results. Interim conclusions are given in Section 7. A full discussion of our findings is deferred to Paper II.

2 THE ASSOCIATIVE IONIZATION REACTION

Associative ionization is the most elementary collisional process by which molecular bonds can be formed. The cross-section for the associative ionization reaction,

$$H + H(2s) \rightarrow H_2^+ + e^-, \quad (12)$$

has been measured as a function of the relative collision energy by Urbain et al. (1991). Although this reaction is endothermic by about 0.75 eV, the measured threshold is ~ 1.1 eV. The cross-section is reproduced in Fig. 1 for the energy range 0.5–1.0 eV (from Urbain et al. 1991). The cross-section peaks at a value of 2.4×10^{-17} cm^2 at the H_2^+ dissociation threshold (3.4 eV). Above this energy the reaction

$$H + H(2s) \rightarrow H + H^+ + e^- \quad (13)$$

becomes competitive. A notable feature is the structure at about 2 eV. This is caused by the total mixing of the two quasi-degenerate channels: H(1s)+H(2s) and

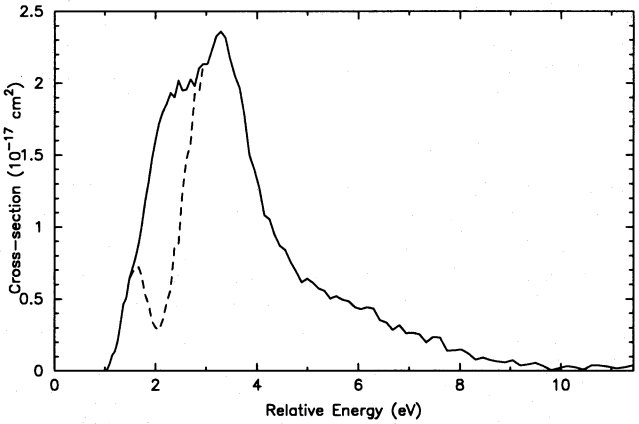

Figure 1. Cross-sections for the associative ionization reaction $H+H(n=2)\rightarrow H_2^+ + e^-$. The dashed line shows the cross-section for the H(2s) channel only (data from Urbain et al. 1991). The solid line is the weighted mean for the 2s and 2p channels.

H(1s)+H(2p). Non-adiabatic transitions occur between these channels when they transform into the hybrids H(2s±2p) (Urbain et al. 1991). Thus one channel is favoured at a time, so that the cross-section for the H(1s)+H(2p) channel fluctuates out of phase with that for H(1s)+H(2s) until the cross-sections merge at about 3 to 3.5 eV. A maximum can be expected at about 2 eV for the H(1s)+H(2p) process (Urbain, private communication). This cannot, as yet, be measured directly owing to the short radiative lifetime of the 2p state. For our purposes, we have assumed that the sum of the 2s and the 2p processes results in a smooth, featureless cross-section. To obtain a total $n=2$ cross-section, we have simply assumed that the 2s and 2p states are populated according to their statistical weights. Thus the 2s and 2p cross-sections are given weightings of 1 and 3 respectively. The resultant cross-section is also shown in Fig. 1.

The rate coefficient for reaction (11) can be calculated by integrating $\langle \sigma v \rangle$ over a Maxwellian speed distribution, in which case

$$k=\left(\frac{8k_{\rm B}T}{\pi\mu}\right)^{1/2}\int_{u=0}^{\infty}\sigma u e^{-u}\,{\rm d}u,$$

where σ is the cross-section, $u=(\mu v^2/2kT)$, μ is the reduced mass ($=\frac{1}{2}m_{\rm H}$) and the other symbols have their usual meanings. In Table 1, we present the calculated rate coefficients for the 2s channel (reaction 12) using the measured cross-sections, for the 2p channel using our inferred cross-sections, and for the $n=2$, weighted-mean cross-section as described above.

The temperature dependences of the rate coefficients are smooth, and fits to them are given by

$$k_{2s}=1.16\times10^{-10}\,T^{-0.07}\,e^{-16941/T}\ {\rm cm^3\ s^{-1}}$$
$$(3800\leq T\leq 21\,800\ {\rm K}),$$
$$k_{2p}=1.19\times10^{-8}\,T^{-0.5}\,e^{-19065/T}\ {\rm cm^3\ s^{-1}}$$
$$(3400\leq T\leq 22\,000\ {\rm K}),$$
$$k_{2s,p}=2.41\times10^{-9}\,T^{-0.35}\,e^{-17829/T}\ {\rm cm^3\ s^{-1}}$$
$$(3000\leq T\leq 22\,000\ {\rm K}).$$

Table 1. Values of the rate coefficient (cm^3 s^{-1}) for the associative ionization reaction (11) for several temperature values. Separate entries are given for the H(2s) and H(2p) substates, as well as for the weighted mean.

Temperature (K)	H(2s)	H(2p)	H(2s,p)
3000	3.1×10^{-13}	4.6×10^{-13}	4.2×10^{-13}
4000	9.9×10^{-13}	1.7×10^{-12}	1.5×10^{-12}
5000	2.1×10^{-12}	3.7×10^{-12}	3.3×10^{-12}
6000	3.6×10^{-12}	6.4×10^{-12}	5.7×10^{-12}
7000	5.3×10^{-12}	9.3×10^{-12}	8.3×10^{-12}
10000	1.11×10^{-11}	1.78×10^{-11}	1.61×10^{-11}
15000	1.69×10^{-11}	2.73×10^{-11}	2.51×10^{-11}

These are accurate to within 10 per cent over the specified temperature ranges.

We can place this associative ionization reaction into a general astrophysical context by considering how its efficiency depends upon the state of the host medium. The endothermicity of the reaction gives it a temperature dependence that is steepest at about 6000 K. At temperatures much below this, the direct radiative association route discussed by Latter & Black (1991, reaction 10 here) may be competitive, but at higher temperatures associative ionization is much more important.

However, the H_2 that is formed is susceptible to photodissociation,

$$H_2+h\nu\rightarrow H+H, \qquad (14)$$

and collisional dissociation,

$$H_2+H\rightarrow H+H+H, \qquad (15)$$

$$H_2+H_2\rightarrow H_2+H+H. \qquad (16)$$

Both these processes are highly excitation-dependent, and so are sensitive to the density and temperature.

Associative ionization is unlikely to compete with the negative-ion route in circumstances in which H^- easily survives (i.e. in cool, neutral gas, well removed from significant radiation sources). However, there may be conditions in which associative ionization (reaction 11) is favoured over the positive-ion radiative association route (reaction 6). Reaction (11) is faster than reaction (6) when

$$\frac{n_2}{n_+}>\frac{k_6}{k_{11}},$$

where n_+ and n_2 refer to the number densities in H^+ and $H(n=2)$ respectively. Over the probable temperature range of interest, $5000\lesssim T\lesssim 10\,000$ K, we find that n_2/n_+ needs to be in excess of $1\text{–}3\times10^{-5}$ for associative ionization to dominate (see Table 2).

Quite specialized conditions are necessary to allow the H I $n=2$ level to be so well populated. In conditions close to LTE, the required $n=2$ population is only achieved at implausibly high total densities (in excess of 10^{12} cm^{-3}). At the densities typical of the situations where H_2 formation is

Table 2. Minimum requirements for the efficiency of associative ionization [$H(n=2)+H \rightarrow H_2^+ + e^-$] to exceed the efficiency of radiative association ($H^+ + H \rightarrow H_2^+ + h\nu$).

T_e (K)	n_2/n_+	Implied n_+/n_{tot} for $b_1 \gtrsim b_2$	$n_e b_2/10^{10}$ (cm^{-3})
5000	2.6×10^{-5}	$\lesssim 8\times10^{-6}$	210
7500	1.6×10^{-5}	$\lesssim 0.034$	3300
10 000	1.4×10^{-5}	$\lesssim 0.67$	16 000

an issue, large departures from LTE are required before associative ionization dominates. From equation (17) and the Saha equation we can obtain the minimum value for the product $n_e b_2$ [using the notation b_i to signify the NLTE departure coefficient for H I ($n=i$)]. These are listed for selected temperatures in Table 2. In environments where the primary energy input to the microstate is the ambient radiation field (e.g. hot-star winds and planetary nebulae), the appropriate NLTE effect may result from a combination of high H I Lyman continuum optical depth and excited-state photoionization, or from the existence of an extremely bright source of Lyα photons. Both cases also require high Lyman-line optical depths. This is also true where non-radiative energy inputs dominate, since high H I ($n=2$) populations are more readily sustained if spontaneous radiative decay of the level is closely matched by absorption. In effect, the most propitious environment for effective associative ionization is likely to be one where $b_1 \gtrsim b_2$. If n_2/n_+ is to exceed $1-3\times10^{-5}$, such an environment typically will be less than half-ionized (see Table 2) and probably cooler than 10 000 K.

A further limitation on the effectiveness of associative ionization is the fragility of the intermediate H_2^+ species. Undiluted, unblocked ultraviolet radiation fields and high free-electron densities are to be avoided if reaction (7) is to complete the H_2 formation process efficiently. The troublesome branching reactions, (8) and (9), are discussed further in Section 3. It is these that inhibit the effective operation of associative ionization in the winds of massive young stellar objects. A formal comparison of the efficiencies of associative ionization and radiative association (reactions 11 and 10 respectively) is not possible owing to the model dependence of the H_2^+ stability.

3 CHEMISTRY OF EXCITED HYDROGEN

If a true assessment is to be made of the importance of reaction (11) and related pathways, we must consider the effects that the excitation of molecular as well as atomic species has on the chemistry. The discussion in this section will be limited to the chemistry of a pure hydrogen gas (a brief discussion of certain processes involving other species included in the chemistry is given in Section 4). At the outset, it should be noted that, with the exception of H_2 and a few other molecules, our knowledge of the chemistry of excited states is typically extremely poor. This is particularly apparent for the photoreactions for which, in many cases, the data are poor even for photodissociation and photoionization from the ground state.

To describe a pure hydrogen gas experiencing a significant degree of excitation in a non-equilibrium environment, the effect of radiation transport on at least a two-level atom must be treated. The generation and transfer of H I Lyα and two-photon emission must be included, both in the treatment of the hydrogen atom and in the photochemistry of the more complex molecular species. The hydrogenic molecular species, H_2 and H_2^+, will exist in vibrationally excited states. Transitions from these states have oscillator strengths and cross-sections for photodissociation that are very different from those out of the ground state. Dissociative recombination and other reactions involving H_2^+ are also sensitive to the degree of vibrational excitation. For the sake of simplicity we do not calculate the populations of the vibrational levels in H_2 or H_2^+. The excited vibrational states of these homonuclear molecules have long radiative-decay lifetimes. For the densities and temperatures that we consider they will be dominated by collisions. It is therefore likely that they will be thermalized at the local gas kinetic temperature. For completeness, we consider the two extremes: (i) where the vibrational levels are thermalized, and (ii) where the H_2^+ is in the ground ($v''=0$) vibrational state.

Many of the reactions influencing the chemistry of hydrogen in astrophysical media have been discussed in previous studies (e.g. Dalgarno & Lepp 1987; see also Janev et al. 1987 for a comprehensive description of the processes in hydrogen–helium plasmas). We include here additional information for those reactions where the above-mentioned effects are likely to be important and which are likely to be important in near-stellar environments – the list is far from complete (even when we restrict the arguments to the hydrogen chemistry) and will be expanded upon in more detail in future work. The reactions that are discussed in this section have been included because they have a bearing on the efficiency of the associative ionization reaction.

3.1 $H + H^+ \rightarrow H_2^+ + h\nu$

The rate coefficient for this radiative association reaction has been calculated by Ramaker & Peek (1976) and others, using classical, semi-classical and quantum techniques. From this work we have obtained the following fit to the rate coefficient:

$$k_6 = \begin{cases} 1.38\times10^{-23}\,T^{1.845} \ \mathrm{cm^3\,s^{-1}} & 200 \le T \le 4000\ \mathrm{K}, \\ -6.157\times10^{-17} + 3.255\times10^{-20}\,T \\ \quad -4.152\times10^{-25}\,T^2 \ \mathrm{cm^3\,s^{-1}} & 4000 \le T \le 32\,000\ \mathrm{K}. \end{cases}$$

It should be noted that these values are lower, particularly at lower temperatures, than those that have sometimes been quoted in the literature (e.g. Dalgarno & Lepp 1987; Glassgold et al. 1989). This could have important implications in some studies.

3.2 $H^- + e^- \rightarrow H + e^- + e^-$

Collisional detachment of the H^- ion is usually omitted from reaction schemes due to the high threshold (0.745 eV) for the reaction. However, it may be significant in high-excitation regions (cf. the threshold for associative ionization) and has been included in our calculations. Data from Massey, Bishop & Gilbody (1969) and Janev et al. (1987) show that the cross-section rises sharply from threshold to a maximum value of about 5×10^{-15} cm^2 at $E\simeq13$ eV, then falls off slowly to 2.8×10^{-15} cm^2 at $\simeq50$ eV. From this we can deduce a rate coefficient of

$$k = 3.02\times10^{-15}\,T^{1.67}\,e^{-2087/T},$$

which is accurate to within 11 per cent over the temperature range $3200\leq T\leq18\,800$ K.

3.3 $H_2(v''\geq0) + h\nu \rightarrow H + H$

The photodissociation of H_2 proceeds along well-known lines. The only two excited Rydberg states that are connected to the ground state ($X^1\Sigma_g^+$) are the $B^1\Sigma_u^+$ and the $C^1\Pi_u$ configurations: excitation into these states, via the Lyman and Werner bands respectively, is followed by fluorescent decay into the vibrational continuum of the ground state, leading to spontaneous radiative dissociation. Oscillator strengths for the transitions between the various vibrational levels in the Lyman and Werner bands were taken from Allison & Dalgarno (1970), assuming that $J'=J''=0$. The probabilities for decay of the vibrational levels of the excited states into the continuum of the ground state were taken from Stephens & Dalgarno (1972).

In standard models of interstellar clouds it is usually quite acceptable to assume that the H_2 is in the $v''=0$ state. However, the oscillator strengths for Lyman transitions out of $X^1\Sigma_g^+$ ($v''=1$) are some 5 to 10 times larger than the corresponding values for the $v''=0$ state. This implies that the photodissociation rate for H_2^* may be up to an order of magnitude larger than for $H_2(v''=0)$. In our models, for the purpose of calculating the photodissociation rate, we have assumed that the H_2 vibrational energy levels are thermalized. Further complications arise in any attempted analysis of the line-shielding function for H_2 (i.e. when self-shielding is important), as then it is necessary to consider transfer in each of the lines for each of the excited vibrational levels. This is probably not a major problem in that it is unlikely that in circumstellar regions the vibrationally excited levels of H_2 will be sufficiently abundant to give optically thick lines. Moreover, for $v''\geq3$ direct photodissociation can occur into the continua of the $B^1\Sigma_u^+$, $C^1\Pi_u$ and $B'^1\Sigma_u^+$ states at wavelengths longer than 911.7 Å (Glass-Maujean 1986). Self-shielding is very much less significant in continuum processes than in lines, but unless the H_2 is highly vibrationally excited this process is relatively unimportant. It has not been included in our models.

3.4 $H_2^* + h\nu \rightarrow H_2^+ + e^-$

Ground-state H_2 cannot be ionized by photons longward of the Lyman limit. However, for $v''\geq4$ this is no longer true. Ford, Kirby-Docke & Dalgarno (1975) have calculated the cross-sections as a function of photon energy for photoionization out of $v''=4$ to 14 into excited (v') levels of H_2^+. The cross-sections are quite small (of the order of 10^{-18} cm^2) and consist of the superposition of step functions, each one corresponding to a different v' level of H_2^+. Thus, for $v''=4$, the threshold is 13.53 eV (for excitation into H_2^+ $v'=0$ only) while, for $v''=9$, ionization can occur into the $v'=3$, 4, 5, 6, 7 and 8 levels of H_2^+. In most cases, ionization is not possible at energies below about 12.8 eV.

If we assume that the H_2 vibrational energy levels are thermalized, then we can calculate a thermally averaged cross-section,

$$\langle\sigma\rangle_T = \sum_v w\sigma_v,$$

where

$$w = \left[\frac{e^{-E_v/kT}}{\sum_v e^{-E_v/kT}}\right].$$

Doing this for several values of the temperature (between about 7000 and 16 000 K), we find that the dependence of the cross-section (for any wavelength) on the temperature can be very roughly treated as linear. We are thus able to perform a linear interpolation of the rate coefficient for any particular temperature. The cross-section has non-negligible values in the wavelength range 912–973 Å (see Table 3).

3.5 $H_2^{+*} + h\nu \rightarrow H^+ + H$

Cross-sections for the photodissociation of H_2^+ out of the ground state and excited vibrational levels were calculated by Dunn (1968) and by Von Busch & Dunn (1972) on the assumption that $J''=1$. Despite being an incomplete description of the dissociation from the excited states, their work clearly shows the fundamental properties of the process. Direct photodissociation of the $1s\sigma_g$ configuration into the vibrational continuum of the $2p\sigma_u$ state results in a smooth wavelength dependence of the cross-section (for $v''=0$), which peaks at around 1100 Å and extends to 2000 Å. The cross-sections for $v''>0$ extend to much greater wavelengths and demonstrate a number (equal to v'') of sharp minima. Argyros (1974) developed a procedure so as to include all contributions from 17 vibrational levels and $0\leq J''\leq8$. The calculations give the excitation temperature dependence of

Table 3. Cross-section for the photoionization of H_2 at several wavelength values and for two values of the vibrational excitation temperature.

λ (Å)	σ (cm^2) at 8000 K	σ (cm^2) at 16 000 K
912.8	8.1×10^{-20}	6.6×10^{-19}
940.1	3.0×10^{-20}	3.9×10^{-19}
960.4	6.8×10^{-21}	1.2×10^{-19}
970.5	1.7×10^{-21}	4.0×10^{-20}
980.6	4.3×10^{-22}	7.7×10^{-21}

the cross-section as a function of wavelength (assuming a Boltzmann population distribution in the vibrational levels). They were performed for temperatures of $2500 < T < 26\,000$ K and wavelengths of $500 \leq \lambda \leq 25\,000$ Å. The results (in fig. 5 of that paper) show that, at low temperatures, $v'' = 0$ dominates and the cross-section is strongly peaked at $\simeq 1200$ Å. At higher temperatures, the peak becomes less pronounced and is shifted longwards. At the highest temperatures, the cross-section is still large at wavelengths of several μm.

In our models we have fitted cubic splines to each of the curves in fig. 5 of Argyros (for different temperatures). We have calculated the rates, and interpolated to obtain the value at any particular temperature. We have also used the data in fig. 1 of Argyros to calculate the rates on the assumption of population of $v'' = 0$ only. The recent work by Sarpal & Tennyson (1993) on the vibrational excitation of H_2^+ by electrons indicates that the vibrational levels of H_2^+ will be thermalized for electron densities in excess of about 50 cm^{-3}, for the temperature range of interest here. This condition is usually satisifed in the circumstellar environments considered in this paper. It is not always true for the nebular regions that are discussed in Paper II.

3.6 $H_2^{+*} + e^- \rightarrow H + H$

The rate coefficient for the dissociative recombination of H_2^+ is also dependent on the vibrational excitation. The cross-sections (for $v'' = 0$) measured by Van der Donk et al. (1991) over the restricted centre-of-mass energy range of 0.01–0.1 eV are larger than predicted by Nakashima, Takagi & Nakamura (1987) over the same range, largely due to the measured window resonances being much narrower than predicted by Nakashima et al. Experimental measurements over a larger range of energies are therefore desirable, but we adopt here the temperature-dependent rates calculated by Nakashima et al., which are in any case significantly larger than the rates fitted by Dalgarno & Lepp (1987) to earlier theoretical calculations. Following Nakashima et al. (1987), we adopt

$$k = \begin{cases} 8.8 \times 10^{-8}/T^{0.29}\ \mathrm{cm^3\ s^{-1}} & \text{for } v = 0, \\ 1.81 \times 10^{-6}/T^{0.5}\ \mathrm{cm^3\ s^{-1}} & \text{for } v = 1, \\ 2.8 \times 10^{-7}/T^{0.66}\ \mathrm{cm^3\ s^{-1}} & \text{for } v = 2. \end{cases}$$

3.7 Collisional dissociation

Collisional dissociation is important for molecules that have a small or zero dipole moment (e.g. CO, H_2, N_2, C_2, O_2). The collisional dissociation of H_2 and CO by H and H_2 proceeds as a multistep process, in which the molecules are excited up the vibrational ladder into the continuum faster than they can radiatively relax into the lower states (e.g. Roberge & Dalgarno 1982). The rates are therefore extremely sensitive to both temperature *and* density. Roberge & Dalgarno (1982) calculated critical densities (below which radiative stabilization of the intermediate vibrational states becomes important). For the reactions

$$H + H_2 \rightarrow H + H + H,$$

$$H + CO \rightarrow H + C + O,$$

the critical densities (at 10 000 K) are 10^4 and 10^{10} cm^{-3} respectively.

In our models we have used parametric fits to the curves in Roberge & Dalgarno (1982) to express the temperature and density dependences of these rates. We have also included the full set of the other (less significant) reactions where the collisional partners are H^+, He or electrons. Where information is not available, we have assumed that the rate coefficient is the same as that for dissociation by hydrogen atoms.

4 FURTHER REACTIONS INVOLVING EXCITED ATOMIC HYDROGEN

In a more speculative vein, we consider the likely role of further reactions, involving excited-state reactants, that are not usually included in models of circumstellar chemistry. Having opened the discussion on the relevance of the associative ionization reaction with $H(n=2)$, we should also mention the corresponding reaction for $H(n=3)$:

$$H + H(n=3) \rightarrow H_2^+ + e^-. \qquad (17)$$

This reaction is exothermic by $\simeq 1.14$ eV, so that, unlike the $H(n=2)$ reaction, there is no threshold for the reaction. On the other hand, the $n=3$ level is $\simeq 1.89$ eV above $n=2$ and will have a correspondingly lower population in nearly all regions of interest. Urbain (private communication) has performed very tentative calculations for the (3s) and (3p) channels. The energy dependence of the cross-section is somewhat complicated, but in general it is relatively large at small energies ($\simeq 1.35 \times 10^{-16}$ cm^2 at 0.01 eV) and falls off at higher energies ($\simeq 7.5 \times 10^{-18}$ cm^2 at 0.24 eV), becoming very small at energies above a few eV ($\simeq 1.7 \times 10^{-18}$ cm^2 at 3 eV). This cross-section is not very large and, because it drops off rapidly at high energies, the implied rate coefficient is perhaps not as large as might be expected:

$$k_{17} \simeq (2.1 \times 10^{-7}/T)\, e^{-7137/T}\ \mathrm{cm^{-3}\ s^{-1}}$$

$$\text{for } 4400 \leq T \leq 22\,000 \text{ K}.$$

On the basis of Urbain's rough cross-section estimates, the implied rate coefficient, over the temperature range 4500–8000 K, is never more than about four times as large as the corresponding rate for the $n=2$ reaction (11), and for temperatures greater than about 8000 K it is actually smaller. In the favourable circumstance of detailed balance (i.e. $b_2 = b_3$) we find that the reaction is negligible at all temperatures of interest. To exceed the corresponding $n=2$ rate, marked population inversion is required (e.g. $b_3/b_2 \gtrsim 15$ at 4500 K, and $\gtrsim 5$ at 20 000 K). Since the $H(n=2)$ process itself is only likely to be significant where $b_1 \geq b_2 \gg 1$, a circumstance inimical to such an inversion, it may be concluded that the $H(n=3)$ process is most unlikely to be significant. The reaction

$$H(n=3) + H \rightarrow H_2 + h\nu \qquad (18)$$

may also need to be considered in certain circumstances, but as yet no data are available.

Urbain, Cornet & Jureta (1992) have measured the cross-section for the reaction

$$H(2s) + H(2s) \rightarrow H_2^+ + e^-, \qquad (19)$$

while Poulaert et al. (1978) have measured, and Urbain et al. (1986) have calculated, the cross-section for the reaction

$$H^+ + H^- \rightarrow H_2^+ + e^-. \quad (20)$$

The values are found to be some 10 to 100 times as large as the calculated values for reaction (11) at the collision energies of interest. However, it is not expected that these reactions will be important, since they will be in direct competition with reactions (11) and (3) respectively. Reaction (20) might have some relevance in ionization interfaces, where the neutral hydrogen abundance is relatively low.

Of greater potential interest is the excited-state analogue of the radiative association reaction (6):

$$H^+ + H(n=2) \rightarrow H_2^+ + h\nu. \quad (21)$$

In regions of moderate ionization, this reaction will compete with the ground-state associative ionization reaction (6) when

$$\frac{n_2}{n_1} > \frac{k_6}{k_{21}}.$$

In more neutral regions, where the associative ionization reaction (11) is important, reaction (21) will compete when

$$\frac{n_+}{n_1} > \frac{k_{11}}{k_{21}}.$$

Preliminary estimates (details to be supplied in Paper II) indicate that k_{21} may be of the order of 4×10^{-13} cm^3 s^{-1} in the temperature range of interest. Thus, for example, at 7000 K the above conditions become $n_2/n_1 > 4 \times 10^{-4}$ and $n_+/n_1 > 20$ respectively. Thus it would seem that reaction (21) may be significant in regions of high ionization. The importance of this reaction will be dealt with in more detail in Paper II.

5 THE CHEMISTRY OF NON-HYDROGENIC SPECIES

The available data relating to all aspects of the chemistry of the excited states of non-hydrogenic species are, in general, very poor. Where possible, we have included the relevant information so that the behaviour of other important simple molecular species (e.g. CO, OH) can be studied, In all cases it should be noted that the uncertainties are very large.

For these reasons we chose to keep the species set small (with few triatomic species or larger), although making the reaction set as comprehensive as possible. For example, in the case of the negative ions we included all possible radiative attachment, photodetachment and mutual neutralization reactions, etc. Close attention was paid to the charge-transfer reactions between atomic species, and a limited number of three-body reactions were included (e.g. Rawlings & Williams 1990). The vibrational states of the products in most reactions are unknown, and we have neglected the possible effects of a non-LTE distribution.

As part of this study, a major reassessment of the photochemistry was undertaken. We have included all possible photodissociation and photoionization channels, including those for molecular ions. We note that many undetected, higher lying channels ($\lambda < 1100$ Å) may exist for poorly studied species. A complete set of the available cross-sections and oscillator strengths for photodissociation, photoionization, etc., was compiled. Where only limited data were available for continuous processes, we have fitted the data with cubic splines. Considerable uncertainty in these cross-sections arises from the assumption that the molecules are in the ground electronic and vibrational states. The vertical excitation potentials of the lower lying Rydberg states of many molecules are often less than 1 eV and can be much less. For example, the singlet ground state $X^1\Sigma_g^+$ of C_2 is separated by just 0.09 eV from the first excited triplet state $a^3\Pi_u$. Transitions between these two states are highly forbidden (Padial, Collins & Schneider 1985), and so significant population of the triplet state will persist down to quite low temperatures and densities.

Another potentially major source of error is the treatment of the radiative transfer in the discrete absorption lines that lead to photodissociation. In an expanding atmosphere a Sobolev-type approximation may be used, provided that the thermal width of the lines is small when compared to the wind velocity. We anticipate that, in the regions we are modelling, no molecular absorption lines will be optically thick (with the possible exception of those of H_2 and CO). Thus, while we pay careful attention to continuous absorption processes in our models, line shielding is treated in an approximate way and is included for these two molecules only, which in any case may be shielded by continuum opacities. The self-shielding functions for CO and H_2 were calculated from the standard (dustless) derivations of Tielens & Hollenbach (1985); see Rawlings (1988) for a further description. The oscillator strengths for CO photodissociation were taken from table 1 of Letzelter et al. (1987). Mamon, Glassgold & Huggins (1988) used these data to formulate an accurate Sobolev treatment of the escape probabilities in cold circumstellar envelopes which are illuminated by the interstellar radiation field. To do so, they performed an average over the rotational states for each molecular band. However, the data in Letzelter et al. are for photodissociation out of the $v'' = 0$ level of the ground state (at a temperature of 300 K). A detailed analysis of the escape probabilities in hot circumstellar environments is thus not possible. In the absence of any other information, in our models we simply used the $v'' = 0$ data.

Where data for photoionization reactions are not available, we have assumed (following van Dishoeck 1988) a flat cross-section of 10^{-17} cm^2 at all energies above the vertical ionization threshold. In all cases it must be remembered that the available data on the products of photolysis reactions are very poor. Moreover, branching ratios for photoreactions are strongly wavelength-dependent.

6 MODELS

In this paper we consider the hydrogen chemistry in the immediate circumstellar environment, focusing on the winds of young stellar objects (YSOs). We present the results of model calculations for three distinct classes of outflow. These are

(1) winds from massive YSOs,
(2) T Tauri winds, and
(3) cool neutral outflows.

In each case we have performed time-dependent chemical calculations. In addition to the reactions discussed in this work we have included basic reactions from the UMIST chemical ratefile (Millar et al. 1991). The column densities N(CO), $N(H_2)$, $N[H(n=2)]$ and N(C) are accurately integrated throughout the outflow, with the two molecular columns being initialized to zero at r_{start}. A simple formulation for the self-shielding for H_2, CO (see Section 5) and the neutral carbon continuum is included. The chemistry includes 41 species involving simple molecules, such as CN, alongside H_2 and CO. The only elements included in the scheme are H, C, N, O, He and the representative low-ionization-potential metal, Na. The same chemistry is used in all of the models.

Calculations were performed in the usual way; that is to say, the differential equations for the chemistry were hard-wired using DELOAD and the integrations carried out with the GEAR package. The basic details of the T Tauri and cool neutral outflow models can be found in earlier publications (Rawlings et al. 1988; Glassgold, Mamon & Huggins 1989, 1991).

We calculated the rates (s^{-1}) for the photoreactions by summing the integrated continuum processes and the contributions from the discrete line processes (see van Dishoeck 1988 for details). These calculations were performed for the spectra, dilution factors and continuum opacities that were relevant to our models. In the first two models described below, carbon and all low-ionization-potential metals are ionized, so that only the hydrogen Lyman and Balmer continuum opacities need to be considered, whereas in the cool wind model most atomic species are assumed to be neutral. For each model and for each photoabsorbing species, we computed the basic photorate before running the chemical integration in the following manner. We subdivided the Balmer continuum into 7–10 wavelength bins spaced at appropriate intervals, and integrated the shielded photorate from the Lyman limit out to the effective photoabsorption threshold. For the case of the cool, neutral wind, in which the UV stellar flux is blocked by neutral metals, we began the integration at the ionization limit of magnesium (1622 Å). We assume here that the opacity at greater wavelengths is dominated by the Balmer continuum. By performing these calculations for different values of the optical depth at the Balmer limit (τ_B), it was then possible to approximate the optical-depth dependence of the rate to a polynomial function for each species. This method was found to be computationally advantageous, and the errors incurred in the fitting process (less than a few per cent) are insignificant compared to the general assumptions concerning alternative opacity sources. In our models we are interested in recombination zones and regions where the $H(n=2)$ level is well populated. Strong Lyα (H I λ1215.16) fluxes may thus be present, and have been included in our photodissociation/ionization rates. Molecules such as OH and H_2O are highly susceptible to Lyα.

6.1 Winds from massive YSOs

Like their unobscured evolved counterparts, the winds associated with massive YSOs are likely to be warm out to large radii, and are certainly dense and fairly well ionized. Radio flux and IR spectral line measurements (e.g. Simon et al. 1981) suggest mass-loss rates of the order of 10^{-7} $M_\odot$ yr^{-1} or greater. Also, the outflow velocities implied by the observed IR line widths are only in the region of 100 km s^{-1} or so (as opposed to $\gtrsim$1000 km s^{-1} for unobscured OB stars). This amounts to a combination of mass-loss rate and outflow velocity that can yield significant Balmer as well as extreme Lyman continuum optical depth in the outflow, if the outflow originates close to the YSO. Blocking of the stellar flux in the Balmer continuum ($\lambda \leq 3646$ Å) has important chemical implications since, in the absence of a significant Lyman continuum flux, photoionization of hydrogen proceeds via the $n=2$ level. As the Balmer continuum optical depth increases, this process is suppressed, and both the $H(n=2)$ population and the neutral hydrogen fraction will be enhanced. In addition, many molecular species (e.g. H_2 and, to an extent, H_2^+) are protected against photodissociation.

In setting up an outflow model for a massive YSO, we borrowed from the models used to describe unobscured OB stars. We assumed spherical symmetry and formulated the dependence of velocity upon radius r in the same way, namely

$$v(r) = v(R_*) + [v_\infty - v(R_*)]\left(1 - \frac{R_*}{r}\right)^\beta,$$

where R_* is the stellar radius and v_∞ is the terminal wind velocity (Castor & Lamers 1979). The velocity-law index, β, is at present a free parameter. A dependence of gas temperature on radius is also required as input to the model. We used the following wind temperature profile based on the OB star wind models of Drew (1989, fit presented in Bunn & Drew 1992):

$$\frac{T_r}{T_*} = 0.79 - 0.51\,\frac{v(r)}{v_\infty}.$$

The emergent radiative energy distribution of the YSO was represented by the calculated spectrum from a Kurucz (1991) model atmosphere. The input parameters of the model are as follows:

(i) stellar radius (R_*) = 4.0×10^{11} cm;
(ii) $R_{start} = 3R_*$;
(iii) $\dot{M} = 1.0 \times 10^{-6}$ $M_\odot$ yr^{-1} or 1.0×10^{-5} $M_\odot$ yr^{-1};
(iv) $v(R_*) = 15$ km s^{-1}, $v_\infty = 150$ km s^{-1}, $\beta = 4$ or $\beta = 1$, and
(v) $T_{eff} = 20\,000$ K, $\log g = 4.0$.

The model of the hydrogen atom assumes that photoionization from the ground state is negligible and that H I Lyα is in detailed balance at least out to R_{start}. Its decoupling at larger radii is described using the Sobolev approximation (see Appendix A for details). One very important, effectively free, parameter in this model is the 'initial' value of the Balmer limit optical depth (and hence b_2). Formally, its value is constrained by the mass-loss rate and the wind-velocity law (more gradual acceleration giving a larger total column and higher optical depth). At radii close to the surface of the star, a full description of the chemistry is impractical in our model owing to the extremely stiff nature of the differential equations which describe the chemical and physical processes. So, in order to estimate the magnitude

and parameter dependence of the Balmer limit optical depth, we performed preliminary calculations for each run in which we integrated n_2 from the stellar surface out to $R_{\rm start}$. In doing this, we assumed a simple hydrogen ionization equilibrium in which Case B recombination balances photoionization from $n=2$ and detailed balance ($b_1=b_2$) holds at all positions. Unsurprisingly, we found that the Balmer continuum opacity is extremely sensitive to the details of the velocity law as well as to mass-loss rate.

In the case of significant Balmer continuum opacity, it becomes necessary to include a term in the radiation field that corresponds to the redistribution of the absorbed Balmer flux. This can be represented by

$$J_{\nu,\rm diff}=\left(\frac{B_\nu}{b_2}\right),$$

where B_ν is the Planck function at the local kinetic temperature. The ionization equilibrium can then be written as

$$4\pi b_2 n_2^* W\int_{\nu_{\rm B}}^{\infty}\sigma_\nu I_* e^{-\tau_\nu}\,d\nu+4\pi n_2^*\int_{\nu_{\rm B}}^{\infty}\sigma_\nu B_\nu\,d\nu=n_e n_+\alpha_{\rm B},$$

where n_2^* is the LTE value of n_2 as defined by the Saha–Boltzmann equation, $\nu_{\rm B}$ is the Balmer limit threshold frequency, B_ν is the Planck function at the local kinetic temperature, I_* is the stellar flux, W is the dilution factor and σ_ν is the atomic cross-section for photoionization of the $n=2$ level. This diffuse-field blackbody term is also included in the calculation of molecular photodissociation and photoionization rates in all of the main models where significant Balmer continuum optical depth accumulates. It should, of course, be noted that, if the Balmer continuum opacity becomes very large, then the two-level + continuum model of the H atom becomes inadequate. This limits us to the consideration of models with relatively sharp wind acceleration and mass-loss rates $<10^{-5}\,{\rm M}_\odot\,{\rm yr}^{-1}$.

The results from the preliminary Balmer continuum calculations (i.e. values of n_1, n_2 and the Balmer limit optical depth, $\tau_{\rm B}$ at $R_{\rm start}$) provide the initial conditions for the main YSO wind chemistry model. For the $\dot{M}=1\times10^{-6}\,{\rm M}_\odot\,{\rm yr}^{-1}$, $\beta=4$ model, the values of $\tau_{\rm B}$ and b_2 at $R_{\rm start}$ are 86 and ~5400 respectively. The formation of H_2 in this model is quite inefficient, despite the excited-hydrogen chemistry. The H_2 fractional abundance peaks at 6×10^{-12} at about $17\,R_*$ where atomic hydrogen recombines, and drops to 10^{-13} by $100\,R_*$. Within $25\,R_*$, H_2 is formed by excited-state radiative association (reaction 10), and at large radii via the ground-state radiative association forming H_2^+ (reaction 6). Molecular hydrogen is destroyed with great efficiency by photodissociation and photoionization at all positions. The fractional population in $H(n=2)$ also drops from 10^{-5} to 10^{-9} over the interval $(10\text{–}100)\,R_*$ as H I Lyα becomes optically thin.

By contrast, when the mass-loss rate is raised to, say, 10^{-5} $\rm M_\odot\,yr^{-1}$ and β is reduced to 1.0, the limit our formalism can handle, the derived H_2 abundance is much higher. In Fig. 2(a), we show the fractional abundances of species as a

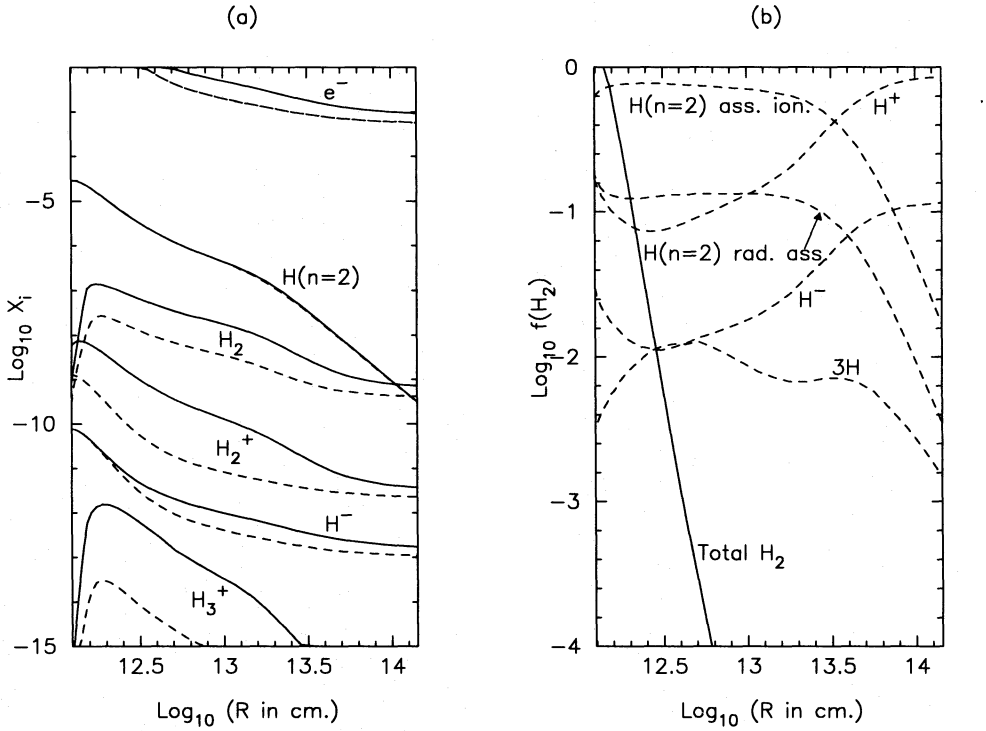

Figure 2. Wind from massive YSO – results for the high mass-loss rate calculations ($10^{-5}\,{\rm M}_\odot\,{\rm yr}^{-1}$). (a) Fractional abundances (X_i) for selected species as a function of radius. The dashed lines show the abundances that are obtained when the associative ionization reaction (11) is not included. (b) H_2 formation rates. The dashed lines show the fractional contribution to the H_2 formation rate as a function of radius for each of the channels discussed in the text. The labelling is: (3H) – three-body (reaction 1), (H^-) – negative ion (reactions 2 and 3), (H^+) – positive ion (reactions 6 and 7), [$H(n=2)$ ass. ion.] – excited-state associative ionization (reactions 11 and 7), and [$H(n=2)$ rad. ass.] – excited-state radiative association (reaction 10). The solid line shows the total H_2 formation rate (arbitrary normalization).

function of radius, calculated with (solid lines) and without (dashed lines) the associative ionization reaction (11) included in the chemistry. In Fig. 2(b), we show the relative contribution to the total H_2 formation rate as a function of radius for each of the channels discussed in this paper. As can be seen from both figures, associative ionization is the dominant channel out to about $80\,R_*$, despite the rapid photodissociation rate for H_2^+. The excited-state radiative association reaction (10) accounts for less than 18 per cent of the H_2 formation rate throughout the wind. The H_2 abundance peaks at 1.4×10^{-7} at a radius of about $4.3\,R_*$. This is a factor of about 6 larger than would be the case if reaction (11) were omitted from the chemistry. The H_2 abundance is limited by photodissociation and collisional dissociation (at large radii). The change in behaviour at high mass-loss rates is attributable to the fact that the $H(n=2)$ population is everywhere greatly enhanced over the $\dot{M}=1.0\times10^{-6}$ $M_\odot$ yr^{-1} case. In fact, hydrogen recombination is forced very early on in the higher $\dot{M}$ model. This is likely to be a somewhat artificial effect due to the absence of $H(n=3)$ and higher levels: a more complete treatment would push the recombination zone out to larger radii and also lower the H_2 abundance somewhat, as a consequence of lowering the $H(n=2)$ population.

The far greater success in producing H_2 via the associative ionization route at the higher mass-loss rate, however, suggests a regime in which very efficient H_2 production might be realized. The most promising ingredients are a combination of high mass-loss rate, an effective temperature $\lesssim 20\,000$ K and, perhaps, gradual acceleration of the outflow. In these circumstances, a high $H(n=2)$ population can be maintained over a large radial range, and there is a greater likelihood of processing the stellar radiation field to less damaging, longer wavelengths via photoabsorption in the Balmer and higher H I bound–free continua.

A test of H_2 production in extremely dense outflows may be provided by the luminous blue variables (early-B hypergiants with mass-loss rates in excess of 10^{-5} $M_\odot$ yr^{-1}). However, medium-resolution 2-μm spectroscopy has so far not revealed any H_2 emission from candidate objects such as η Car (Allen, Jones & Hyland 1985) or MWC 349 (Hamann & Simon 1986, the evolutionary status of this object being especially uncertain). McGregor, Hyland & Hillier (1988) and McGregor, Hillier & Hyland (1988) have detected strong circumstellar CO 2.3-μm overtone vibrational emission from a number of luminous evolved B supergiants in the southern Milky Way and in the LMC, but no accompanying H_2 emission was detected in their medium-resolution 2-μm spectra.

6.2 T Tauri winds

For the case of T Tauri winds, we have adapted the model of Rawlings et al. (1988) to accommodate the new chemistry. The species set is the same as used in the previous models. The wind is both hot (10^4 K) and excited (with an excitation/ionization temperature peaking at $\geq 15\,000$ K). The physical basis of this model is described in Hartmann, Edwards & Avrett 1982; the wind is heated and accelerated as a result of the deposition of energy and momentum by Alfvén waves generated in the stellar convection zone. Terminal velocity and maximum temperatures are reached at about $(3–5)\,R_*$. Radiative cooling (Hartmann et al., fig. 1 and table 1) and adiabatic cooling are both important; hence the wind temperature drops from an initial value of 10^4 K at $5\,R_*$ to 2900 K at $10\,R_*$ and 310 K at $50\,R_*$. In our model the cooling law is expressed in differential form and is integrated along with the chemistry. Other parameters are

$T_{\rm eff}=4000$ K (blackbody),

$R_*=2.0\times10^{11}$ cm,

$n=5.0\times10^8$ cm^{-3} at $r=5\,R_*$,

$v_\infty=230$ km s^{-1}.

The initial ionization was calculated from the balance of recombination and collisional ionization. The mass-loss rate is small ($\simeq 5\times10^{-9}$ $M_\odot$ yr^{-1}), and the cooling rate is large. The Balmer continuum optical depth is therefore low at all times. Since the wind is largely neutral ($\simeq 50$ per cent ionization at $5\,R_*$ dropping to 4 per cent at $100\,R_*$), the Lyman continuum is opaque. In the outer parts of the wind the C I ionization continuum and the H_2 and CO absorption lines which lead to photodissociation may also be optically thick.

Results from a model in which detailed balance ($b_1=b_2$) holds everywhere are given in Figs 3(a) and (b). From these figures, it can be seen that the importance of the associative ionization is limited to within $0.1\,R_*$ of the starting radius ($5\,R_*$) and even then has a marginal significance (accounting for just 8 per cent of the total H_2 formation rate – see Fig. 3b), although it may be more important inside the starting radius. The reason for this is straightforward – because of the high excitation temperature and the (relatively) low densities, the H_2^+ is more rapidly destroyed by the IR radiation field than by charge exchange (reaction 7) to form H_2. H^- is also suppressed by the radiation field. In these circumstances, direct excited-state radiative association (reaction 10) is more important and results in a significant enhancement of H_2 by a factor of about 7 within a few R_* (with corresponding enhancements in the abundances of other species, e.g. H_3^+, OH, OH^+, HCO^+, CH, etc.). At radii greater than this, the net effects of the $H(n=2)$ reactions become insignificant, and ground-state radiative association of H_2^+ (reaction 6) becomes the dominant H_2 formation channel. This is to be expected due to the rapid fall in the temperature [and hence in the $H(n=2)$ population – see Fig. 3(a)].

In models where we have relaxed the condition that $b_1=b_2$ and assume that the Case B approximation is applicable, we obtain much the same result. In these cases, the $H(n=2)$ population is initially lower ($b_2<b_1$), since the density is not sufficiently high for Lyα to be optically thick, even at the base of the wind. Further out, $b_2>b_1$ due to dynamical effects, but the rapid decline in the temperature strongly inhibits the associative ionization reaction. The principal H_2 destruction route is by collisional dissociation – hence the sharp rise in the abundances of H_2 and associated species when the temperature drops. We note that, within a few R_*, CO, C_2, O_2 and several other simple molecular species are also formed by direct radiative association and thus are not coupled to the H_2 formation routes.

6.3 Cool neutral outflows

Lizano et al. (1988) detected a high-velocity H I outflow from the young stellar outflow system SVS 13/HH7-11. They

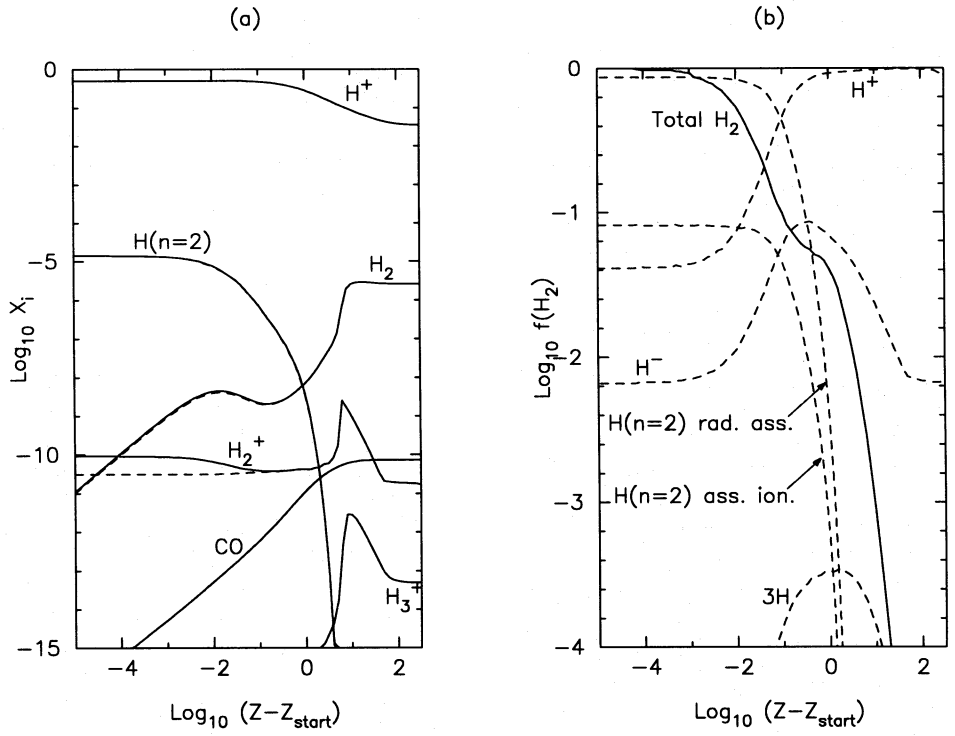

Figure 3. T Tauri wind. (a) Fractional abundances (X_i) for selected species as a function of the radial coordinate $Z\,(=r/R_*)$. (b) Relative contribution to the total H_2 formation rate for each of the formation channels discussed in the text as a function of Z – see Fig. 2 for a description of the labelling.

determined a terminal velocity of 170 km s^{-1} and a mass-loss rate of 3×10^{-6} $M_\odot$ yr^{-1}. The stellar source is estimated to have a luminosity of 50 $L_\odot$ and an effective temperature of 5000 K. Carr & Tokunaga (1992) obtained high-resolution spectra of the CO overtone emission bands at 2.3 μm from SVS 13 and, by fitting the $v=2$–0 band head with an LTE slab model, estimated a rotational temperature of 3000–4500 K.

In the dense, cool, neutral winds associated with low-mass YSOs, such as SVS 13/HH7-11, there can be no significant Lyman continuum radiation and ground-state collisional ionization will be unimportant. Hence the n_2/n_+ ratio is determined by the balance between Case B recombination and photoionization out of the $n=2$ state, while the n_2/n_1 ratio is fixed by the balance of collisional excitation against de-excitation and net radiative decay (calculated as described in Appendix A). In the inner wind, where Lyα is extremely optically thick, detailed balance ($b_1=b_2$) holds. Further out, the lower density and Lyα optical depth will eventually lead to depopulation of the $n=2$ level.

In order to test the importance of the associative ionization reaction and the other reactions discussed in this paper, we have investigated two models for the outflow from SVS 13 that are much like those considered by Glassgold et al. (1989; 1991 Case 2). As our purpose is solely to examine the potential role of excited-state processes in H_2 formation, we do not attempt a detailed comparison with these earlier calculations here. We name our models I and II, and list the key physical input parameters in Table 4.

In both models, the outflow is spherically homogeneous and the young star is assumed to radiate like a blackbody. Since carbon, sulphur, silicon, magnesium and iron are all neutral in the wind, there is attenuation of the continuum radiation at wavelengths <1622 Å which is taken into account. Consequently, there is little direct H_2 or CO dissociating flux. Since the aluminium is ionized alongside sodium, we crudely allow for this by raising the abundance of sodium, our representative low-ionization-potential metal, to 3.56×10^{-6}. The populations of H^+, $H(n=2)$ and $H(n=1)$ are in statistical equilibrium at Z_0. The oxygen and nitrogen ionizations are initially set to the equilibrium established by charge exchange, namely $(O/O^+)=\frac{9}{8}(H/H^+)$ and $(N/N^+)=\frac{2}{9}(H/H^+)$.

In model I the H_2 is mainly created by three-body formation (reaction 1) within $2R_*$. Between about $2R_*$ and $20R_*$ it is formed by three-body reaction and the H^+ route (reactions 6 and 7) with comparable efficiencies. Further out, the H^- route dominates. At no stage does either excited-state radiative association (reaction 10) or the associative ionization route (reactions 11 and 7) account for more than about 1 per cent of the total H_2 formation rate. H_2 is destroyed by collisional dissociation and reactions with C, O and O^+ (to form CH, OH and OH^+). The insignificance of both excited-state processes is a consequence of the low $n=2$ fractional abundance imposed by the low wind temperatures ($T\leq5000$ K): at its highest at the base of the wind, this abundance is only 2.5×10^{-10} (or $b_2\sim5$).

The major change in the specification of model II with respect to that of model I is the replacement of constant outflow velocity by a law that allows the outflow to accelerate up to terminal velocity (see Table 4). Since the chosen velocity law is clearly unphysical as $Z=r/R_*\rightarrow1$, the calcula-

Table 4. Physical parameters used in the cool stellar wind models.

	Model I		Model II
$T_{\rm eff}$	5000 K		5000 K
R_*	5×10^{11} cm		6.63×10^{11} cm
$Z_0 (= r_0/R_*)$	1.0		1.055
$v(r)$	150 km s^{-1}		$[1-(R_*/r)]\times 150$ km s^{-1}
$\dot{M}$	3×10^{-6} M$_\odot$ yr^{-1}		3×10^{-6} M$_\odot$ yr^{-1}
$T_{\rm ej}(r)$	5000 K	($Z<2$)	5000 K
	5000 (2/Z) K	($Z>2$)	

tion is started at $Z_0 = 1.055$ where the outflow velocity is equal to the adiabatic sound speed (this follows the practice of Ruden, Glassgold & Shu 1990, who also used this velocity law). At this starting radius the density is much higher than in model I (2×10^{13} cm^{-3} as compared with 2×10^{12} cm^{-3}). However, as the temperature is still set at 5000 K, the H($n=2$) fractional abundance is unchanged. Hence again the reactions involving H($n=2$) are practically negligible throughout the wind. The difference is that the high densities close to the base of the wind allow the three-body reaction (1) to dominate H_2 formation – further out the (H^+, H_2^+) channel becomes significant. The principal H_2 loss routes are collisional dissociation (by H atoms), and reactions with C and O to form CH and OH. At $Z=375$, $X(H_2)=2\times10^{-8}$, $X(CO)=3\times10^{-7}$. In contrast to this, 'Case 2' of Glassgold et al. (1991, hereafter GMH91) gave $X(H_2)=1.5\times10^{-3}$ and $X(CO)=4\times10^{-4}$.

Our model II paints a much gloomier picture regarding the efficiency of H_2 production than is suggested by its closest parallel in GMH91, even though the two use the same density profile. It is interesting to consider in general terms why this is so. The key difference lies in the assumed radial dependences of the temperature. GMH91 used the temperature profile derived by Ruden et al. (1990), in which the gas temperature drops sharply from its initial value of 5000 K to about 1100 K within $Z<2$ – thereafter the temperature continues to decline, but much more slowly. Since most of the constructive chemistry relating to H_2 formation in Case 2 of GMH91 occurs very close to the star, where densities are very high, the effect of the greatly reduced temperature within a stellar radius or so is to freeze in the consequences of this through severe limitation of many of the destructive chemical pathways at large radii (e.g. collisional dissociation of H_2). The adoption of constant temperature in our model II has undoubtedly allowed these destructive processes to undo the H_2 synthesis achieved in the inner wind – however, the peak abundances inferred from model II in the proximity of the star would not be significantly affected by this.

Just as the destruction of H_2 is clearly very temperature-sensitive, so also is its creation via the excited-state processes (10 and 11). To illustrate both of these effect, we have run model II with the gas kinetic temperature increased arbitrarily to 7500 K (Fig. 4). The H I $n=2$ fractional abundance is then over three orders of magnitude higher at radii where Lyα remains in detailed balance ($b_1=b_2\simeq90$) and non-negligible Balmer continuum optical depth accumulates. In this setting the associative ionization H_2 formation route is dominant out to about 35 R_*, where the H^+ route (reaction 6) takes over. Indeed, despite the enhanced collisional dissociation rate at the higher temperature, the H_2 abundance is higher by a factor of about 3 (within 20 R_*) as compared to the cooler model. Further out, the $n=2$ population declines, the H_2 formation rate falls and the enhanced collisional dissociation rate reduces the asymptotic H_2 abundance by a factor of about 7 relative to the cooler model. The lesson from GMH91 is that, had a sharp decline been imposed on the temperature profile after the initial synthesis of H_2 by associative ionization, this process could have left its mark on the asymptotic H_2 abundance.

We conclude that the outflow from SVS 13 is too cool for excited-state routes to H_2 to be significant. However, the strong positive temperature dependence of the associative ionization process in particular does carry the implication that it may have an important role to play in slightly warmer environments.

7 CLOSING REMARKS

The calculated rate coefficients for the associative ionization reaction involving excited hydrogen atoms ($n=2$) are over 50 times as large (for $T\geq4000$ K) as the rates for the corresponding direct radiative association reaction (Latter & Black 1991). Although the relative efficiency of H_2 formation largely depends on the subsequent stability of the H_2^+ ion, associative ionization is more significant in most regions of astrophysical interest. Large departures from LTE [i.e. large H($n=2$) populations] are required for either reaction to be important.

A fuller description of the molecular and atomic excitation is essential in the environments where these reactions are likely to be significant. Most of the astrochemical literature quote rate coefficients that are only applicable to the ground state (as is usually appropriate in the interstellar medium). In general, the rate coefficients for the excited vibrational states of molecules are larger than for the ground state.

A full overview of the results obtained in both this paper and Paper II is deferred to the end of Paper II.

ACKNOWLEDGMENTS

We are grateful to Dr X. Urbain for correspondence and access to unpublished calculations on associative ionization reactions by excited hydrogen atoms. We thank Dr J. Tennyson for sharing his knowledge on molecular hydrogen systems, and Drs B. Sarpal and J. Tennyson for access in advance of publication to their electron – H_2^+ collision cross-section calculations. We also thank Dr G. Mamon for his

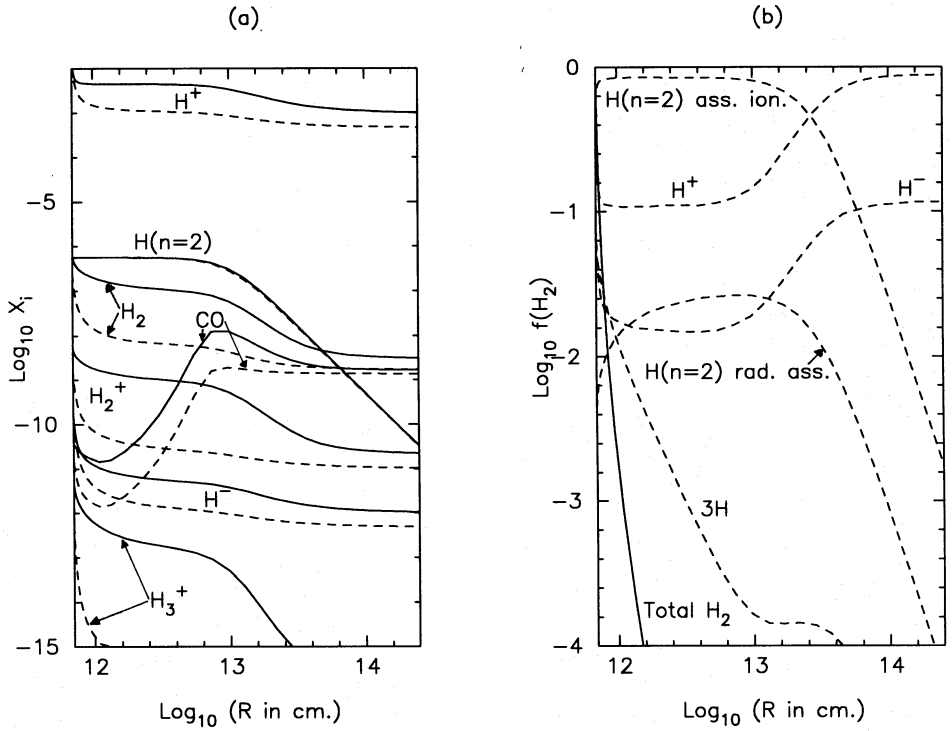

Figure 4. Neutral, massive outflow – model II with T(gas) = 7500 K. (a) Fractional abundances (X_i) for selected species as a function of radius. (b) Relative contribution to the total H_2 formation rate for each of the formation channels discussed in the text as a function of radius – see Fig. 2 for a description of the labelling.

detailed and constructive comments on this paper. JMCR and JED acknowledge support from SERC fellowships.

REFERENCES

Allen D. A., Jones T. J., Hyland A. R., 1985, ApJ, 291, 280
Allison A. C., Dalgarno A., 1970, At. Data, 1, 289
Argyros J. D., 1974, J. Phys. B, 7, 2025
Bunn J. C., Drew J. E., 1992, MNRAS, 255, 449
Carr J. S., Tokunaga A. T., 1992, ApJ, 393, L67
Castor J. I., 1970, MNRAS, 149, 111
Castor J. I., Lamers H. G. J. L. M., 1979, ApJS, 39, 481
Dalgarno A., Lepp S., 1987, in Vardya M. S., Tarafdar S. P., eds, Astrochemistry. Reidel, Dordrecht, p. 109
Drew J. E., 1989, ApJS, 71, 267
Dunn G. H., 1968, Phys. Rev. (2nd series), 172, 1
Ford A. L., Kirby-Docken K., Dalgarno A., 1975, ApJ, 200, 788
Giovanardi C., Natta A., Palla F., 1987, A&AS, 70, 269
Glassgold A. E., Mamon G. A., Huggins P. J., 1989, ApJ, 336, L29
Glassgold A. E., Mamon G. A., Huggins P. J., 1991, ApJ, 373, 254 (GMH91)
Glass-Maujean M., 1986, Phys. Rev. A, 33, 342
Hamann F., Simon M., 1986, ApJ, 311, 909
Hartmann L., Edwards S., Avrett E., 1982, AJ, 261, 279
Janev R. K., Langer W. D., Evans K., Jr, Post D. E., Jr, 1987, Atoms and Plasmas Vol. 4: Elementary Processes in Hydrogen-Helium Plasmas. Springer–Verlag
Johnson L. C., 1972, ApJ, 174, 227
Kurucz R. L., 1991, Stellar Atmospheres: Beyond Classical Models. NATO ASI series C, Vol. 341, Kluwer, Dordrecht, p. 441
Latter W. B., Black J. H., 1991, ApJ, 372, 161
Letzelter C., Eidelsberg M., Rostas F., Breton J., Thieblemont B., 1987, Chem. Phys., 114, 273
Lizano S., Heiles C., Rodriguez L. F., Koo B.-C., Shu F. H., Hasegawa T., Hayashi S., Mirabel I. F., 1988, ApJ, 328, 763
McGregor P. J., Hillier D. J., Hyland A. R., 1988, ApJ, 334, 639
McGregor P. J., Hyland A. R., Hillier D. J., 1988, ApJ, 324, 1071
Mamon G. A., Glassgold A. E., Huggins P. J., 1988, ApJ, 328, 797
Massey H. S. W., Bishop E. H. S., Gilbody H. B., 1969, Electronic and Ionic Impact Phenomena, Vol. 1. Oxford Univ. Press, Oxford, p. 158
Millar T. J., Rawlings J. M. C., Bennett A., Brown P. D., Charnley S. B., 1991, A&AS, 87, 585
Nakashima K., Takagi H., Nakamura H., 1987, J. Chem. Phys., 86, 726
Padial N. T., Collins L. A., Schneider B. I., 1985, ApJ, 298, 369
Poulaert G., Brouillard F., Claeys W., McGowan J. W., Van Wassenhove G., 1978, J. Phys. B, 11, L671
Ramaker D. E., Peek J. M., 1976, Phys. Rev. A, 13, 58
Rawlings J. M. C., 1988, MNRAS, 232, 507
Rawlings J. M. C., Williams D. A., 1990, MNRAS, 246, 208
Rawlings J. M. C., Williams D. A., Cantó J., 1988, MNRAS, 230, 695
Rawlings J. M. C., Drew J. E., Barlow M. J., 1992, in Singh P. D., ed., Proc. IAU Symp. 150, The Astrochemistry of Cosmic Phenomena. Kluwer, Dordrecht
Roberge W., Dalgarno A., 1982, ApJ, 255, 176
Ruden S. P., Glassgold A. E., Shu F. H., 1990, ApJ, 361, 546
Sarpal B. K., Tennyson J., 1993, MNRAS, 263, 909
Seaton M., 1958, MNRAS, 118, 504
Simon M., Righini-Cohen G., Felli M., Fischer J., 1981, ApJ, 245, 552
Stephens T. L., Dalgarno A., 1972, J. Quant. Spectrosc. Radiat. Transfer, 12, 569

Tielens A. G. G. M., Hollenbach D., 1985, ApJ, 291, 722
Urbain X., Giusti-Suzor A., Fussen D., Kubach C., 1986, J. Phys. B, 19, L273
Urbain X., Cornet A., Brouillard F., Giusti-Suzor A., 1991, Phys. Rev. Lett., 66, 1685
Urbain X., Cornet A., Jureta J., 1992, J. Phys. B, 25, L189
Van der Donk P., Yousif F. B., Mitchell J. B. A., Hickman A. P., 1991, Phys. Rev. Lett., 67, 42
van Dishoeck E., 1988, in Millar T. J., Williams D. A., eds, Rate Coefficients in Astrochemistry. Kluwer, Dordrecht, p. 49
Von Busch F., Dunn G. H., 1972, Phys. Rev. A, 5, 1726

APPENDIX A: THE HYDROGEN ATOM

For the sake of simplicity, we have adopted a model of the hydrogen atom which has two levels plus the continuum. With the assumption of an on-the-spot-type approximation we do not include recombination to the ground state. Case B recombination rate coefficients are calculated from the formalism of Seaton (1958), which gives the temperature dependence over the range 1000–20 000 K.

Electron impact excitation (C_{12}) and hence de-excitation (C_{21}) rates for $n=2$ are calculated from the tables in Giovanardi, Natta & Palla (1987). Thus

$$C_{12}=\frac{8.63\times10^{-6}\,\upsilon e^{-E_{\rm th}/k_{\rm B}T}}{g_{\rm nl}\sqrt{T}},$$

where $E_{\rm th}$ is the threshold energy, $g_{\rm nl}$ is the statistical weight of the initial state, and υ is the effective collision strength. Giovanardi et al. give third-order polynomials for $\upsilon(T)$ for the 1s–2s and 1s–2p transitions. We have used a weighted average (in the ratio 1:3) to obtain the net values for the 1–2 transition. We also include collisional de-excitation by hydrogen atoms and, following Ruden et al. (1990), we make the simplifying assumption that the rates for hydrogen atom excitation are $(m_{\rm e}/m_{\rm H})^{1/2}$ times the values for excitation by electrons.

Collisional ionization is not likely to be significant, but is included for the sake of completeness. The temperature dependence of ionization from the ground and $n=2$ states (C_{1+} and C_{2+}) is calculated from the formulae given in Johnson (1972).

The photoionization rates for $n=1$ and 2 (Γ_{1+} and Γ_{2+}) are calculated by integrating the cross-sections for these processes over the appropriate radiation field. This takes into account the relevant continuum optical depths (as discussed in the main text) and the dilution factor for the radiation field, W, given by

$$W=\tfrac{1}{2}[1-\sqrt{1-(r_*^2/r^2)}],$$

where r and r_* are the wind and stellar radii respectively.

A1 Ly α transfer

Bearing in mind the large uncertainties in both the physics and the chemistry of the regions that we are studying, a full treatment of the radiative transfer is not yet justified. We describe here a simplified form of the Sobolev approximation for the transfer of radiation in outflows.

The radiation bracket which describes the transition rate between the $n=2$ and $n=1$ levels can be written as $A_{21}\beta$, where β is the net escape probability in the Ly α line. Note that the B_{12} term is implicitly included in this radiation bracket.

In an expanding atmosphere, the optical depth in the line can be written as

$$\tau_0=\frac{\pi e^2}{m_{\rm e}c}f_{12}\lambda n_1\frac{r}{\upsilon} \tag{A1}$$

(Castor 1970), where f_{12} and λ are the oscillator strength and wavelength for Ly α (0.4162 and 1215.16 Å respectively), n_1 is the number density of H($n=1$), and r and υ are the wind radius and velocity. Stimulated emission is negligible in our applications, and so no correction has been made for it. At large optical depths, the escape probability β tends towards the limit

$$\beta=\frac{1}{\tau_0}. \tag{A2}$$

In the case of a constant-velocity, spherically symmetric wind, we can define a direction-dependent optical depth,

$$\tau(\mu)=\frac{\tau_0}{1-\mu^2}, \tag{A3}$$

where $\mu=\cos\theta$ and θ is the angle between the photon path and the outward radial direction. The escape probability as a function of μ is given by

$$\beta(\mu)=\frac{1-e^{-\tau(\mu)}}{\tau(\mu)}. \tag{A4}$$

Noting that in the cases of interest the mass-loss rates are high ($\simeq10^{-6}$ M$_\odot$ yr^{-1}) and the terminal velocities are low ($\upsilon_\infty\leq100$ km s^{-1}), we can crudely correct the Castor (1970) formalism for a finite thermal speed (which is non-negligible compared to the outflow velocity) and use it to define a range of μ wherein escape in a single flight is possible:

$$\beta=\int_0^{\mu_{\rm max}}\frac{1-e^{-\tau(\mu)}}{\tau(\mu)}\,{\rm d}\mu, \tag{A5}$$

where

$$\mu_{\rm max}=1-\frac{\upsilon_{\rm th}}{\upsilon}=\mu_*, \tag{A6}$$

and $\upsilon_{\rm th}$ and υ are the thermal and wind velocities respectively. In the case of large τ_0, this leads to the following modified expression for the escape probability which is used in our calculations:

$$\beta=\mu_*\left[1-\frac{\mu_*^2}{3}\right]\frac{1}{\tau_0}. \tag{A7}$$

This expression is valid wherever $(\mathrm{d}\ln v/\mathrm{d}\ln r) \ll 1$, and τ_0 is large. In practice, our calculations usually start some distance away from the stellar surface, where both of these conditions are satisfied. The one exception is in the cool stellar wind model (after GMH91), for which the calculations start very close to the photosphere where acceleration is still occurring. In that case, the standard Sobolev approximation as presented in Castor (1970) is used, with the μ^2 term in equation (A3) replaced by $\mu^2(1 - \mathrm{d}\ln v/\mathrm{d}\ln r)$.